Doublet Lattice-Source Method for Calculating Unsteady Loads on Cavitating Hydrofoils

James F. Unruh*
Boeing Commercial Airplane Company, Seattle, Wash.
and
Robert L. Bass III†
Southwest Research Institute, San Antonio, Texas

An approximate solution to the linearized coupled integral equations describing the unsteady loads generated by harmonically oscillating finite span partially cavitating hydrofoils is presented. A doublet lattice-source method is utilized which is an extension of the doublet lattice method used to solve the corresponding fully wetted flow lifting surface integral equation. The advantage of the doublet lattice-source method of solution lies in its ability to accurately represent the lift and moment distributions of geometrically complex partially cavitating hydrofoils without prior knowledge of the behavior of the differential pressure or source strength distributions. Numerical results for life and moment coefficients obtained by the doublet lattice-source method compare well to exact solutions for the limiting case of high-aspect ratio partially cavitating hydrofoils and to existing numerical results for supercavitating finite aspect ratio hydrofoils.

Nomenclature

b = reference length, usually foil root semichord
c = foil chord, also subsurface chord
h = box semi-width, also heave displacement
i = an index, also complex number, $\sqrt{-1}$
j = an index
k = an index, also reduced frequency $k = \omega b/U$
l = an index, also a subscript denoting leading edge of foil
p = perturbation pressure; nondimensional with respect to ρU^2
Δp = differential pressure across the foil
$\langle p(\xi,\eta)_\rho \rangle$ = jump in $\partial p/\partial \rho$ across the foil
q_{ij} = generalized forces
t = a subscript denoting trailing edge
w = upwash on the soil surface
x,y,z = Cartesian coordinates of a field point
C_L = coefficient of lift
C_M = coefficient of moment
D_{ij} = influence function
E = distance in percent foil chord from foil leading edge to initiation of cavity
$H(x-\xi)$ = unit step function
I = unit diagonal
I_1 = modified Bessel function of the first kind order one
K_1 = modified Bessel function of the third kind order one
L_1 = modified Struve function of order one
NWW = number of boxes on the wetted surface
NWC = number of boxes on the cavitating surface
NCC = number of boxes on the trailing cavity
P_c = cavity pressure
P_∞ = freestream pressure
R = radius vector from field point to a point on the foil
S = foil surface area
U = freestream velocity in the x-direction
α = foil angle of attack
$\delta(y-\eta)$ = unit delta function
ξ,η,ρ = Cartesian coordinates of a point on the foil
μ = sweep angle
π = mathematical constant, 3.14159265 . . .
ρ = fluid density
σ = cavitation number
ω = oscillatory frequency

Received May 13, 1974; revision received July 1, 1974. This work was sponsored under the General Hydrodynamics Research Program by the Naval Ship Research and Development Center, Department of the Navy, Washington, D.C. under Contract N00014-73-C-0075.

Index categories: Hydrodynamics; Aeroelasticity and Hydroelasticity.

*Specialist Engineer, Acoustics Research Staff.

†Manager, Hydro-Mechanical Systems, Department of Mechanical Sciences.

Introduction

THE upsurge in the use of hydrofoil craft to gain greater speeds in marine transportation requires a corresponding increase in the understanding of the hydrofoil steady and unsteady loads to insure the performance and structural integrity of hydrofoil designs. For example, lift modulation with flaps provides a means of control and load alleviation for both surface-piercing and submerged-foil systems and the design of a load alleviation or suppression system depends on an accurate prediction of the unsteady loads on cavitating hydrofoils. An initial contribution to the basic understanding of unsteady loads on cavitating hydrofoils was due to Woods.[1] By using the theory of complex potentials and hodograph transformations, a mathematically rigorous solution was obtained; however, the results were limited to infinite aspect ratio foils at a zero cavitation number. Even though considerable theoretical guidance for the development of 2-D cavitating foils have become available[2-5] since Wood's contribution, the effects of finite aspect ratio have been given relatively little attention.

Widnall[6] and Nishiyama and Miyamoto[7] have approached the finite aspect ratio hydrofoil using a fully linearized, 3-D potential approach. In these works pressure doublets are used to represent the foil surface and pressure sources to represent the cavity. These pressure singularities are applied on the central plane of the linearized hydrofoil-cavity system, in the same way as in the corresponding 2-D linearized theory. The formulation results in a system of integral equations for the unknown strengths of the singularity distributions. Widnall assumed a set of elementary pressure functions and a series of source functions based on the corresponding 2-D hydrofoil distributions and solved for the unknown functions' coefficients through a collocation procedure at a finite number of points on the foil-cavity and trailing cavity surfaces. Results were obtained in steady flow for fully cavitating foils at nonzero cavitation numbers and in unsteady flow at the steady cavity pressure. Likewise, Nishiyama and Miyamoto carried out a steady-state lifting surface approximation based on the known 2-D supercavitating singularity distributions and while neglecting gravity effects, took into account the free surface by an image method. For the fully submerged steady-state supercavitating hydrofoil, the results of these two approaches agree reasonably well. For the prediction of unsteady loads on supercavitating hydro-

foils, Widnall's approach appears to work quite well; however, the choice of pressure and source functions relies on knowledge of the corresponding 2-D hydrofoil pressure and source strength distributions. This approach has a definite drawback if one wishes to consider a general configuration hydrofoil, such as a partially cavitating finite aspect ratio hydrofoil with sweep, taper, and a trailing edge control surface. In this paper a method is presented that has the capability, within the limits of linearized theory, to predict the unsteady loads on a general configuration cavitating hydrofoil.

Governing Equations

The linearized formulation of the integral equations[6] relates the normal velocity (upwash) on the hydrofoil surface [$w(x,y) = \partial z(x,y)/\partial x + ikz(x,y)$, where $z(x,y)$ is the hydrofoil displacement distribution] to the pressure jump across the foil surface, $\Delta p(\xi,\eta)$, and to the jump in the normal derivative of the pressure on the cavity surface, $\langle p(\xi,\eta)_\rho \rangle$, by

$$w(x,y)\big|_{Sww+Swc} = \int\int_{Sww+Swc} \Delta p(\xi,\eta)\bar{\mathbf{K}}_1(x-\xi, y-\eta, k)d\xi d\eta + \int\int_{Swc+Scc} \langle p(\xi,\eta)_\rho \rangle \bar{\mathbf{K}}_2(x-\xi, y-\eta, k)d\eta \quad (1)$$

The cavity pressure P_c is related to $\Delta p(\xi,\eta)$ and $\langle p\ (\xi,\eta)_\rho \rangle$ by

$$-(1/2)\sigma(x,y)\big|_{Swc+Scc} = \int\int_{Swc} \Delta p(\xi,\eta)\bar{\mathbf{K}}_3(x-\xi, y-\eta)d\xi d\eta + \int\int_{Swc+Scc} \langle p(\xi,\eta)_\rho \rangle \bar{\mathbf{K}}_4(x-\xi, y-\eta)d\xi d\eta \quad (2)$$

where σ is the cavitation number defined by $\sigma = (P_\infty - P_c)/q$, P_∞ is the freestream pressure and q the dynamic pressure. It should be pointed out that linearized theory is valid only if $\sigma \ll 1$ and it is generally assumed that for small amplitude unsteady motion the cavity pressure, P_c, remains unchanged from its steady value, hence $\sigma = 0$ for $k \gtrless 0$.

The relations of Eq. (2) are satisfied on the projection of the foil and cavity in the x-y plane as shown in Fig. 1. The distance Ec is the point aft of the leading edge where the cavity is assumed to initiate and c is the foil chord. Sww, Swc, and Scc denote, respectively, the foil wetted surface, the foil surface with cavity, and the trailing cavity surface.

The kernel functions of the integral relations are

$$\bar{\mathbf{K}}_1(x-\xi, y-\eta, k) = \{\exp[-ik(x-\xi)]/[4\pi(y-\eta)^2]\} \times \{\beta K_1(\beta) - i\beta + i\pi\beta[I_1(\beta) - L_1(\beta)]/2 + (x-\xi)\exp[ik(x-\xi)]/\sqrt{(x-\xi)^2 + (y-\eta)^2} - i\beta\int_0^{k(x-\xi)/\beta} \tau \exp[i\beta\tau]/\sqrt{1+\tau^2}\,d\tau\} \quad (3)$$

where $\beta = k|y-\eta|$, $I_1(\beta)$ and $K_1(\beta)$ are modified Bessel functions of the first and third kind of order one and $L_1(\beta)$ is the modified Struve function of order one.[8] The kernel function $\bar{\mathbf{K}}_1$ is the kernel function for fully wetted incompressible flow which has been given much attention in the field of aeroelasticity.[9]

$$\bar{\mathbf{K}}_2(x-\xi, y-\eta, k) = -(1/2)\exp[-ik(x-\xi)]H(x-\xi)\delta(y-\eta) \quad (4)$$

where $H(x-\xi)$ is the unit step function and $\delta(y-\eta)$ a delta function.

$$\bar{\mathbf{K}}_3(x-\xi, y-\eta) = -(1/2)\delta(x-\xi)\delta(y-\eta) \quad (5)$$

and

$$\bar{\mathbf{K}}_4(x-\xi, y-\eta) = 1/[4\pi\sqrt{(x-\xi)^2 + (y-\eta)^2}] \quad (6)$$

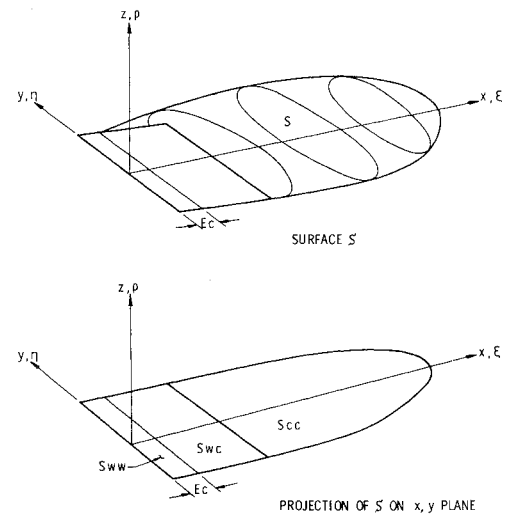

Fig. 1 Closed surface of the cavity and foil and its projection on the x, y plane.

In the case of finite cavity flows, various methods have been proposed to account for the trailing edge of the cavity. The concern with specifying a trailing edge condition stems from the fact that the constant pressure condition on the cavity prevents the occurrence of a stagnation point with smooth flow off the trailing edge. Nishiyama and Myamoto[7] used a semi-closed model for the cavity wherein the cavity length specified an open width at the cavity termination. Other cavity closure models have been proposed such as the re-entrant jet model, modified Riabouchinsky model, and smooth wake termination model.[6] All these closure conditions result in a cavity termination constraint equation to the coupled integral equations. In the present development the cavity is terminated by requiring the pressure source strength to go to zero beyond the cavity trailing edge. This termination condition is particularly attractive since it does not require a constraint equation to further complicate the numerical solution of the coupled integral equations. It should, however, be pointed out that imposing a constraint equation for a more realistic cavity termination condition will not effect the validity of the present method and results from this program indicate that the more relaxed condition used herein will not effect the validity of the results for hydrofoils with trailing cavities in excess of one chord length.

Method of Solution

The present solution technique differs from that of previous researchers[6,7] in that no prior knowledge of the distributions of the pressure source strengths $\langle p(\xi,\eta)_\rho \rangle$ or differential pressures $\Delta p(\xi,\eta)$ are required to determine these unknown distributions. The key element to circumventing an assumed distribution approach is the use of the doublet lattice[10] numerical method of unsteady subsonic aerodynamics to carry out the integral of $\bar{\mathbf{K}}_1$ in Eq. (1). In the doublet lattice method, the lifting surface is divided into small trapezoidal boxes arranged in columns parallel to the freestream and so that surface edges lie on or near box boundaries (see Fig. 2). The ¼ chord line of each box contains a distribution of acceleration potential doublets of uniform but unknown strength to represent the unsteady pressure field and a bound horseshoe vortex whose "bound" portion coincides with the doublet line to represent the steady pressure field of the box, as is shown in Fig. 3. The doublet line and bound vortex of each box produces a normal velocity field proportional to the box pres-

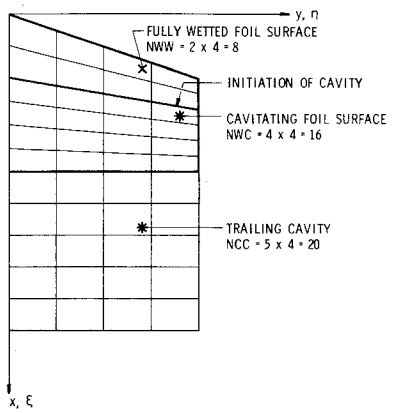

Fig. 2 Typical box pattern for a partially cavitating hydrofoil.

sure at all planform boxes, giving rise to an influence function of the form

$$w(x_D, y_D)_i = \sum_{j=1}^{NWW+NWC} D_{ij}\Delta p_j(\xi_Q, \eta_C) \tag{7}$$

The normal velocities $w(x_D,y_D)$ are collocated at all box midspan ¾ chord locations to yield the $\Delta p(\xi_Q,\eta_C)$ distribution which is considered to be constant across each box evaluated at the box ¼ chord midspan location.

The D_{ij} influence function consists of two major contributions, that due to the bound steady-state vortex as described by Hedman[11] via the Biot-Savart law and that due to the unsteady doublet line as described by Albano and Rodden.[10] The mathematical development of the influence function D_{ij} is well documented in Refs. 10–12 and will not be repeated herein. In order to enhance the integrations required by the D_{ij} influence function, the steady-state vortex of Hedman was retained for the oscillatory representation and the steady part ($k = 0$) of $\bar{\mathbf{K}}_1$ was removed prior to the integrations.

The doublet lattice box scheme is extended to the cavity regions on the foil and trailing cavity. The $\langle p(\xi,\eta)_\rho \rangle$ distribution is represented as a distribution of monopole sources of unknown strength across the cavity surfaces. The second term of Eq. (1) involves the integration of the kernel $\bar{\mathbf{K}}_2$ and the $\langle p(\xi,\eta)_\rho \rangle$ distribution across the cavitating portion of the foil surface. The source distribution is taken to be constant across each box at its value at the box center (ξ_C,η_C). This results in an additional contribution to the normal velocity of the form

$$w(x_D, y_D)_i = \sum_{m=1}^{NWC} S_{im}\langle p_m(\xi_C, \eta_C)\rangle \tag{8}$$

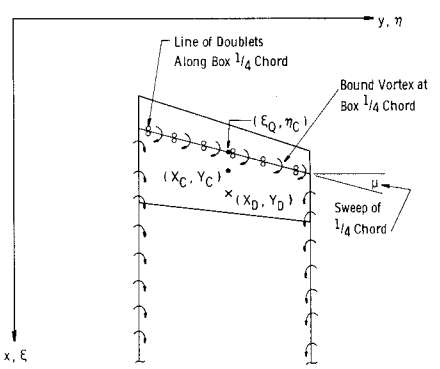

Fig. 3 Typical box acceleration potential doublet line and bound horseshoe vortex geometry.

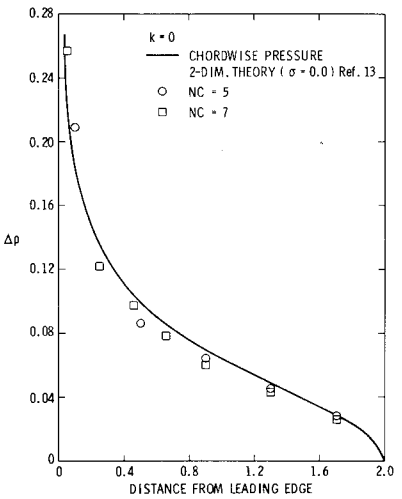

Fig. 4 Pressure distribution on inboard chord of an aspect ratio 6 fully cavitating hydrofoil.

where

$$S_{im} = \begin{cases} 0 & \eta_C \neq y_D \\ 0 & x_D < \xi_l \\ i\{1 - \exp[ik(\xi_l - x_D)]\}/2k & \xi_l < x_D < \xi_t \\ i\{\exp[ik(\xi_t - x_D)] - \exp[ik(\xi_l - x_D)]\}/2k & x_D > \xi_t \end{cases} \tag{9}$$

and the source box leading and trailing edges are ξ_l and ξ_t, respectively.

Thus, the total contribution to the normal velocity distribution across the foil surface takes the form

$$w(x_D, y_D)_i = \sum_{j=1}^{NWW+NWC} D_{ij}\Delta p_j(\xi_Q, \eta_C) + \sum_{m=1}^{NWC} S_{im}\langle p_m(\xi_C, \eta_C)\rangle \tag{10}$$

where the summations over i and j are over all foil boxes and the summation over m is over all source boxes on the foil surface.

The contribution of $\Delta p(\xi,\eta)$ to the cavity pressure is given by the first expression of Eq. (2) wherein the integration of the kernel $\bar{\mathbf{K}}_3$ and the $\Delta p(\xi,\eta)$ distribution is carried out over all cavity boxes on the foil. The resulting integration yields

$$-(1/2)\sigma(x_C, y_C)_l = -\frac{1}{2}\Delta p_l(\xi_C, \eta_C) = -(1/2)\Delta p_l(\xi_Q, \eta_C) \tag{11}$$

since the pressure across each box is taken to be constant at its value at the box ¼ chord midspan location (ξ_Q,η_C).

The second integral of Eq. (2) yields the influence of the source distribution $\langle p(\xi,\eta)_\rho \rangle$ on the cavity pressure distribution $\sigma(x,y)$ and is written as a source influence function

$$-(1/2)\sigma(x_C, y_C)_l = \sum_{m=1}^{NWC+NCC} R_{lm}\langle p_m(\xi_C, \eta_C)_\rho\rangle \tag{12}$$

The influence function R_{lm} is given by

$$R_{lm} = 4\pi \int\int_{\text{box } m} 1/[(x_C - \xi)^2 + (y_C - \eta)^2\ ]^{1/2} dS \tag{13}$$

where l and m vary over all cavity boxes. The integration for R_{lm} across a trapezoidal box is straightforward; however, it is a rather lengthy expression and is given in de-

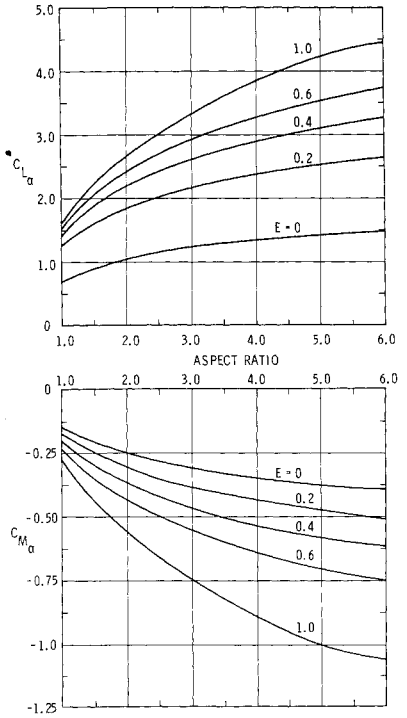

Fig. 5 ***Lift and moment*** **coefficient due to** ***pitch*** **of a partially cavitating foil for various values of** E **(**$k = 0$**).**

tail in an Appendix of Ref. 12. The total contribution to the cavity pressure is given by

$$-(1/2)\sigma(x_C, y_C)_i = -(1/2)\Delta p(\xi_Q, \eta_C) + \sum_{m=1}^{NWC+NCC} R_{lm}\langle p_m(\xi_C, \eta_C)_\rho\rangle \quad (14)$$

The matrix form of Eqs. (10) and (14) is given by

$$\begin{Bmatrix} w_i \\ \hline w_j \\ \hline -\sigma_m/2 \\ \hline -\sigma_\eta/2 \end{Bmatrix} = \left[\begin{array}{c|c|c|c} D_{11} & D_{12} & 0 & 0 \\ \hline D_{21} & D_{22} & S_{23} & 0 \\ \hline 0 & -I/2 & R_{33} & R_{34} \\ \hline 0 & 0 & R_{43} & R_{44} \end{array}\right] \begin{Bmatrix} \Delta p_i \\ \hline \Delta p_j \\ \hline \langle p_\rho\rangle_m \\ \hline \langle p_\rho\rangle_\eta \end{Bmatrix} \begin{array}{l} \text{on } Sww \\ \\ \text{on } Swc \\ \\ \text{on } Swc \\ \\ \text{on } Scc \end{array} \quad (15)$$

where the system of equations are in partitioned form to pointout the coupling between the lift distribution Δp and the source distribution $\langle p_\rho \rangle$. The system of equations is of order $N \times N$ where N is given by $N = NWW + 2*NWC + NCC$ and NWW is the number of fully wetted boxes on the foil surface, NWC the number of foil boxes with a cavity (the cavitating portion of the foil) and NCC the number of boxes in the trailing cavity. Solutions for the Δp and $\langle p_\rho \rangle$ distributions can be obtained by direct inverse of the influence matrix. With the Δp distribution known, the forces moments generated by the upwash and cavitation pressure can be computed directly.

Numerical Results

The numerical accuracy of the present method is demonstrated in the results to follow wherein comparisons of pressures, lifts, and moments on the most inboard chord of an aspect ratio 6 foil are made with the 2-D results of Guerst[13] and Woods.[1] Low-aspect-ratio results are checked by comparison to those results obtained by Widnall[6] for a supercavitating aspect ratio 1 foil.

The versatility of the present method is shown in the results presented for partially cavitating foils wherein the

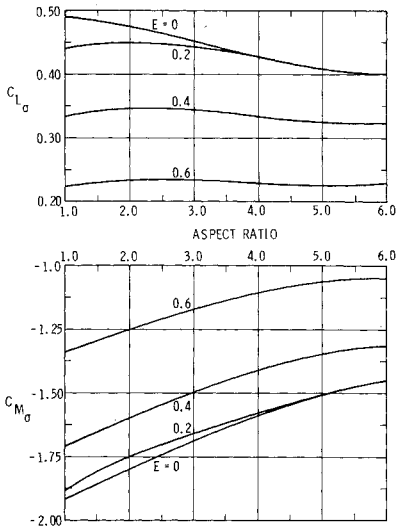

Fig. 6 ***Lift and moment*** **coefficient due to** ***cavitation*** **number of a partially cavitating foil for various values of** E **(**$k = 0$**).**

distance from the leading edge of the foil to the initiation of the cavity, E, is varied (E is given in percent chord). Convergence to the case of fully wetted flow is clearly demonstrated when E approaches unity, hence when the cavity is no longer on the foil.

Throughout the results to follow, a trailing cavity of three chord lengths was used. It was found by Widnall[6] and verified by the authors that the foil lifts and moments are insensitive to trailing cavity lengths beyond three chords and therefore the minimum length was chosen to reduce computer time.

The box patterns for the foils used in the following analyses generally consisted of, unless otherwise noted, eight to ten boxes along the foil chord with seven boxes along the trailing cavity chords. There were six spanwise boxes used on the aspect ratio 4 and 6 foils and five spanwise boxes on the aspect ratio 1 and 2 foils.

Steady Flow Results

In Fig. 4 the chordwise pressure distribution on the most inboard chord of an aspect ratio 6 supercavitating foil ($E = 0.0$) is compared with the 2-D pressure distribu-

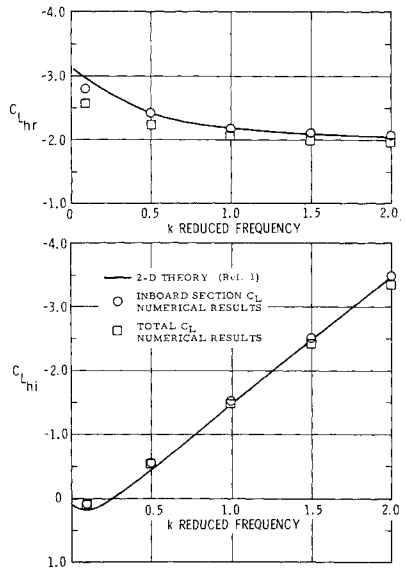

Fig. 7 ***Lift*** **coefficient due to** ***heave for an aspect ratio 6*** **partially cavitating foil comparison with 2-D theory,** $E = 0.2$.

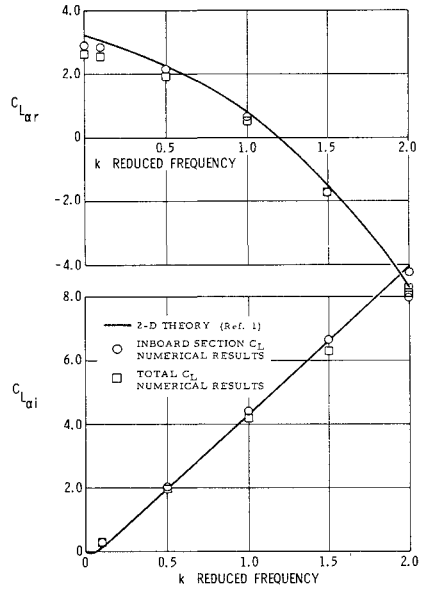

Fig. 8 *Lift* coefficient due to *pitch* for an *aspect ratio 6* partially cavitating foil comparison with 2-D theory, E = 0.2.

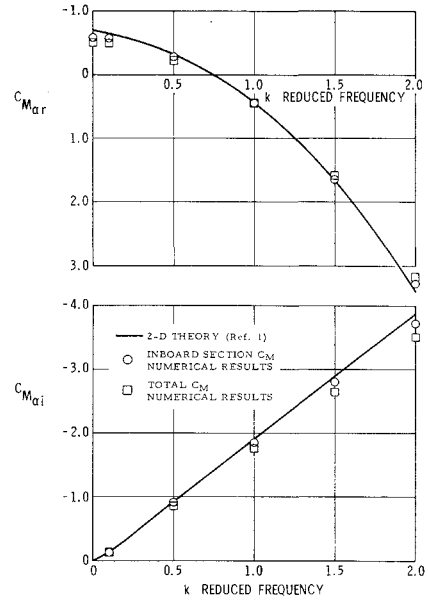

Fig. 10 *Moment* coefficient due to *pitch* for an *aspect ratio 6* partially cavitating foil comparison with 2-D theory, E = 0.2.

tion given by Guerst.[13] The hydrofoil box pattern consisted of six spanwise boxes on the foil halfspan (NS = 6) with five and seven boxes on the foil chord (NC = 5 and NC = 7) and seven chordwise boxes along the trailing cavity. The present method appears to be well converged at NC = 7. The difference between the 2-D results and the present method can be attributed to aspect ratio effects.

For a given foil geometry and length of cavity, the unknown distributions are linear functions of W and σ and the generated lifts and moments can be put into coefficient form and written as

$$C_L = C_{L_\alpha} \times \alpha + C_{L_\sigma} \times \sigma$$

and (16)

$$C_M = C_{M_\alpha} \times \alpha + C_{M_\sigma} \times \sigma$$

where the upwash is expressed in terms of the foil angle of attack ($w = -\alpha$). The contributing force and moment coefficients are nondimensionalized with respect to the foil surface S, the freestream dynamic pressure q, foil chord $2b$ for the moment coefficient and the foil angle of attack α or cavitation number σ.

The effects of aspect ratio and partial cavitation on the lift and moment coefficients due to pitch and cavitation number are shown in Figs. 5 and 6. As can be seen the coefficients uniformly converge to the fully wetted flow case (E = 1.0) as the cavity separation point is moved aft on the foil. Also shown is the effect of aspect ratio on the coefficients. The effect of aspect ratio on $C_{L(\alpha)}$ and $C_{M(\alpha)}$ is more pronounced with increasing values of E, hence with a more aft initiation of the cavity, while the $C_{L(\sigma)}$ and $C_{M(\sigma)}$ exhibit an opposite trend with increasing E; however, the trend is not as pronounced.

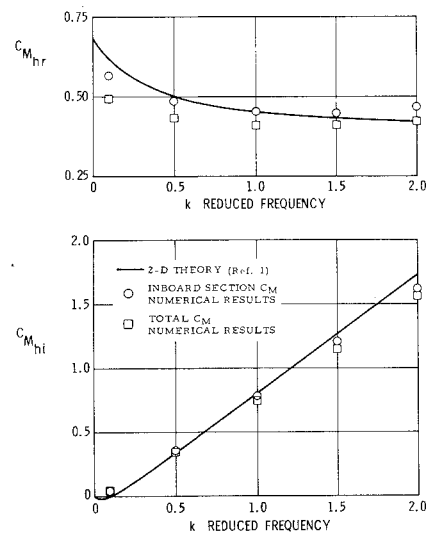

Fig. 9 *Moment* coefficient due to *heave* for an *aspect ratio 6* partially cavitating foil comparison with 2-D theory, E = 0.2.

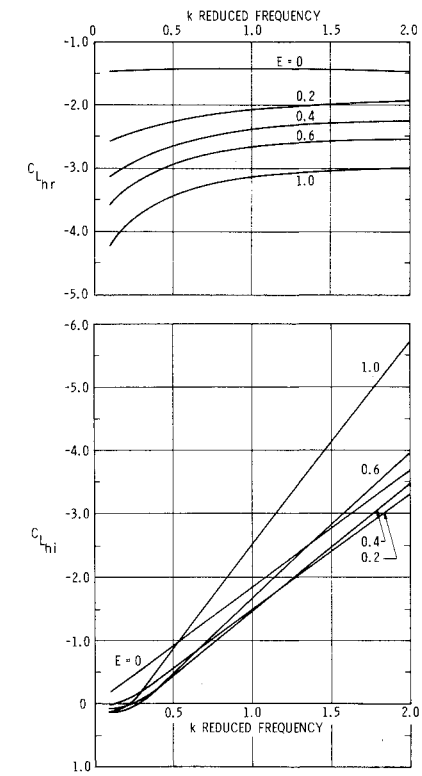

Fig. 11 *Lift* coefficient due to *heave* for an *aspect ratio 6* partially cavitating foil for various values of E.

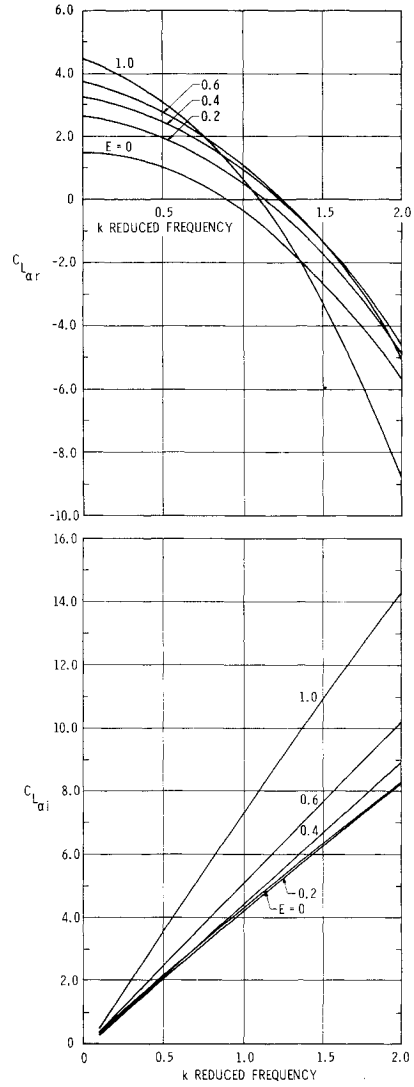

Fig. 12 *Lift* coefficient due to *pitch* for an *aspect ratio 6* partially cavitating foil for various values of *E*.

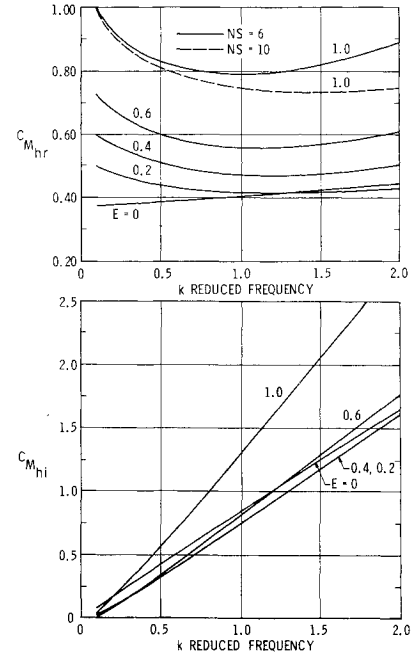

Fig. 13 *Moment* coefficient due to *heave* for an *aspect ratio 6* partially cavitating foil for various values of *E*.

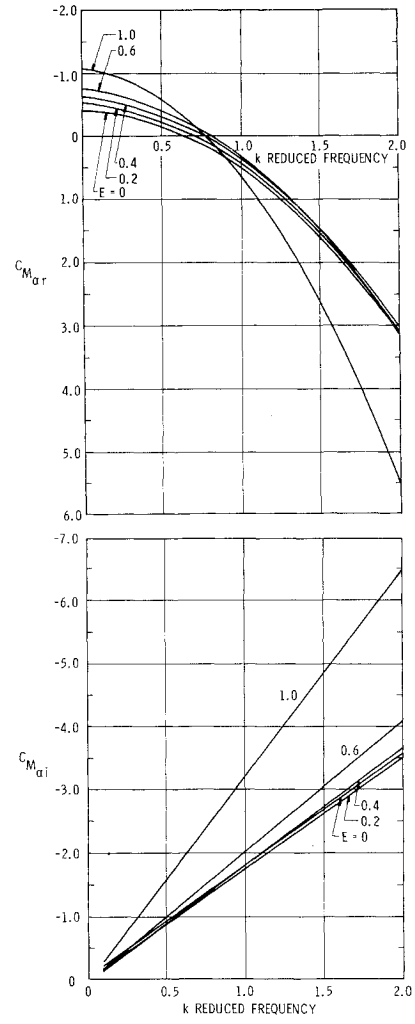

Fig. 14 *Moment* coefficient due to *pitch* for an *aspect ratio 6* partially cavitating foil for various values of *E*.

Oscillatory Flow Results

The validity of the doublet lattice representation for the oscillatory contribution to the lift and moments on cavitating hydrofoils was first checked by comparing the un-

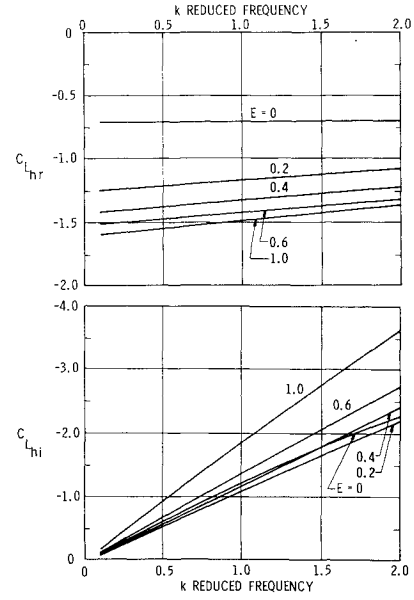

Fig. 15 *Lift* coefficient due to *heave* for an *aspect ratio 1* partially cavitating foil for various values of *E*.

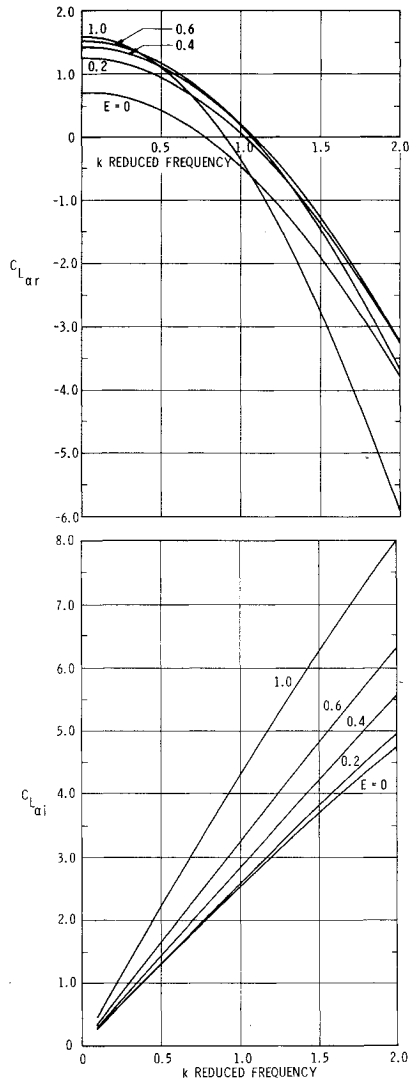

Fig. 16 ***Lift*** **coefficient due to** ***pitch*** **for an** ***aspect ratio 1*** **partially cavitating foil for various values of** ***E.***

steady hydrodynamic coefficients for the most inboard section of an aspect ratio 6 foil in heave and pitch about

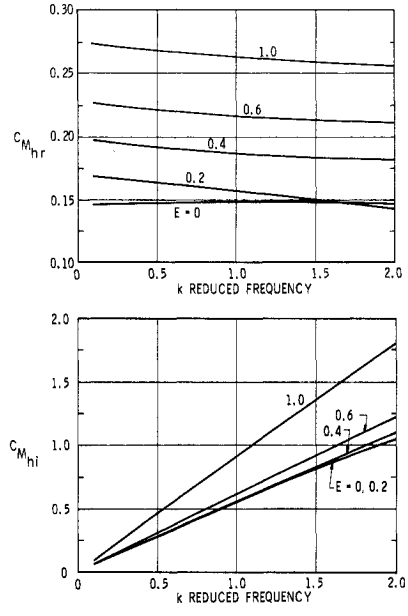

Fig. 17 ***Moment*** **coefficient due to** ***heave*** **for an** ***aspect ratio 1*** **partially cavitating foil for various values of** ***E.***

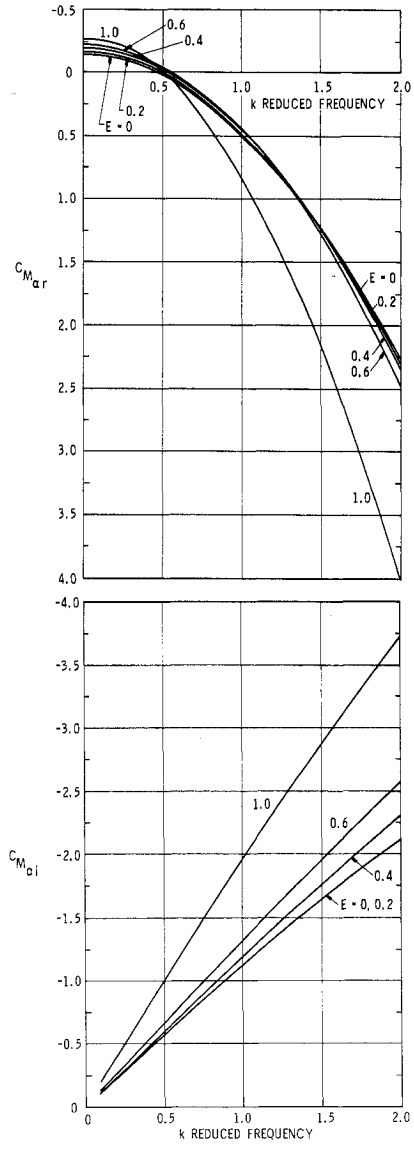

Fig. 18 ***Moment*** **coefficient due to** ***pitch*** **for an** ***aspect ratio 1*** **partially cavitating foil for various values of** ***E.***

the leading edge to the 2-D results as predicted by Woods.[1] The unsteady coefficients for $E = 0.2$ are plotted vs reduced frequency k in Figs. 7–10. The lift and moments coefficients about the foil leading edge have the following definitions:

$$\begin{aligned} C_{L_{hr}} + C_{L_{hi}} &= \text{lift due to heave}/(ikqSh) \\ C_{L_{\alpha r}} + C_{L_{\alpha i}} &= \text{lift due to pitch}/(qS) \\ C_{M_{hr}} + C_{M_{hi}} &= \text{moment due to heave}/(ikqS2bh) \\ C_{M_{\alpha r}} + C_{M_{\alpha i}} &= \text{moment due to pitch}/(qS2b) \end{aligned} \tag{17}$$

where q is the dynamic pressure, h the heave displacement, α the pitch angle, b the semi-chord, and S the foil section area or foil total area for finite aspect ratio results. The present method agrees quite well with the 2-D results. Similar results were obtained for $E = 0.0$, 0.4, and 0.6 and may be found in Ref. 12.

In Figs. 11–14 the total lift and moment coefficients for an aspect ratio 6 foil are plotted vs reduced frequency for various values of E. The convergence to the fully wetted flow case ($E = 1.0$) is apparent. In Fig. 13 the total coefficient $C_{M(hr)}$ demonstrates a sensitivity to spanwise convergence with the trend being more pronounced with increasing values of k and E, a similar trend was shown by

the sectional coefficient. The values of all other coefficients were effectively unchanged with an increase in spanwise boxes.

The lift and moment coefficients for an aspect ratio 1 supercavitating foil exhibit good agreement with the numerical results of Widnall,[6] the detailed comparisons are given in Ref. 12. Lift and moment coefficients for the supercavitating aspect ratio 1 foil and the effects of moving the cavity initiation point aft are shown in Figs. 15–18. Here we may again note the convergence of the method to the fully wetted flow case when E approaches 1.0.

Conclusions

A general numerical approach to the prediction of unsteady loads on cavitating hydrofoils has been developed through the use of a doublet lattice-source representation. Extensive comparisons were made to the 2-D results of Woods for both supercavitating and partially cavitating foils at high-aspect ratios. Finite-aspect-ratio results compare well with existing numerical approaches for the supercavitating foil and numerical results for partially cavitating foils are presented. In view of the results obtained, the method, within the limits of linearized theory, has been shown to be a valid approximation to the solution of unsteady loads on cavitating hydrofoils.

The advantage of the doublet lattice-source method lies in the ability of the method to represent the behavior of the lift distributions of geometrically complex partially cavitating hydrofoils without special regard to the behavior of the differential pressure or source strength distributions.

References

[1]Woods, L. C., "Aerodynamic Forces on an Oscillating Aerofoil Fitted with a Spoiler," *Proceedings of the Royal Society of London,* Vol. 239, Ser. A, No. 1218, March 1957, pp. 328–337.

[2]Parkin, B. R., "Fully Cavitating Hydrofoils in Nonsteady Motion," Rept. 85-2, July 1957, Engrg. Div., Calif. Inst. of Tech., Pasadena, Calif.

[3]Martin, M., "Unsteady Lift and Moment on Fully Cavitating Hydrofoils at Zero Cavitation Number," *Journal of Ship Research,* Vol. 6, No. 1, June 1962, pp. 15–25.

[4]Chu, W. H., "Linearized, Oscillating, Supercavitating Flow at Non-Zero Cavitation Number," Tech. Rept. 1, Contract NObs-90344, 1964, Southwest Research Inst., San Antonio, Texas.

[5]Wang, D. P. and Wu, T. Y., "General Formulation of a Perturbation Theory for Unsteady Cavity Flows," *Journal of Basic Engineering, Transactions of the ASME,* Ser. D, Vol. 87, No. 4, Dec. 1965, pp. 1006–1010.

[6]Widnall, S. E., "Unsteady Loads on Supercavitating Hydrofoils of Finite Span," *Journal of Ship Research,* Vol. 10, No. 2, June 1966, pp. 107–118.

[7]Neshiyama, T. and Miyamoto, Y., "Lifting-Surface Method for Calculating the Hydrodynamic Characteristics of Supercavitating Hydrofoil Operating Near the Free Water Surface," Tech. Rept., Tohoku Univ., Sendai, Japan, Vol. 34, No. 2, 1969.

[8]Abramowitz, M. and Stegun, I. A., *Handbook of Mathematical Functions,* Applied Mathematics Ser. 55, 1965, National Bureau of Standards, Washington, D.C.

[9]Watkins, C. E., Runyan, H. L., and Woolston, D. S., "On the Kernel Function of the Integral Equation Relating the Lift and Downwash Distributions of Oscillating Finite Wings at Subsonic Speeds," Rept. 1234, 1955, NACA.

[10]Albano, E. and Rodden, W. P., "A Doublet Lattice Method for Calculating Lift Distributions on Oscillating Surfaces in Subsonic Flows," *AIAA Journal,* Vol. 7, No. 2, Feb. 1969, pp. 279–285.

[11]Hedman, S. G., "Vortex Lattice Method for Calculation of Quasi Steady State Loadings on Thin Elastic Wings in Subsonic Flow," Aeronautical Research Institute of Sweden, Stockholm, Rept. 105, 1965.

[12]Unruh, J. F. and Bass, R. L., "A General Theory of Unsteady Loads on Cavitating Hydrofoils," Rept. SR 023 01 01, 1974, Southwest Research Institute, San Antonio, Texas.

[13]Guerst, J. A., "Linearized Theory of Two Dimensional Cavity Flows," doctoral dissertation, 1961, Techn. Hogeschool, Delft, The Netherlands.